remote sensing

MDPI

Article

Evaluating Coseismic Landslide Susceptibility Following the 2022 Luding Earthquake: A Comparative Analysis of Six Displacement Regression Models Integrating Epicentral and Seismogenic Fault Distances within the Permanent-Displacement Framework

Tianhao Liu [1], Mingdong Zang [1,2,*], Jianbing Peng [1,2] and Chong Xu [3,4]

[1] School of Engineering and Technology, China University of Geosciences (Beijing), Beijing 100083, China; tianhao.liu@email.cugb.edu.cn (T.L.); dicexy_1@126.com (J.P.)
[2] Institute of Geosafety, China University of Geosciences (Beijing), Beijing 100083, China
[3] National Institute of Natural Hazards, Ministry of Emergency Management of China, Beijing 100085, China; chongxu@ninhm.ac.cn
[4] Key Laboratory of Compound and Chained Natural Hazards Dynamics, Ministry of Emergency Management of China, Beijing 100085, China
* Correspondence: mzang@cugb.edu.cn

Abstract: Coseismic landslides have the potential to cause catastrophic disasters. Thus, it is of crucial importance to conduct a comprehensive regional assessment of susceptibility to coseismic landslides. This study rigorously interprets 13,759 coseismic landslides triggered by the 2022 Luding earthquake within the seismic zone. Employing the Newmark method, we systematically assess the susceptibility to coseismic landslides through the application of six distinct displacement regression models. The efficacy of these models is validated against the actual landslide inventory using the area under the receiver operating characteristic (ROC) curve. A hazard map of coseismic landslides is generated based on the displacement regression model with the highest degree of fit. The results show that Moxi Town, Detuo Town, the flanks of the Daduhe River, Wandonghe River, Hailuogou River, and Yanzigou River are high-susceptibility areas for coseismic landslides. This study explores factors influencing model fit, revealing that the inclusion of the epicentral distance and the distance to the seismogenic fault in displacement prediction enhances model performance. Nevertheless, in close proximity to fault zones, the distance to the seismogenic fault exerts a more significant influence on the spatial distribution density of coseismic landslides compared to the epicentral distance. Conversely, in regions situated further from fault zones, the epicentral distance has a greater impact on the spatial distribution density of coseismic landslides compared to the distance to the seismogenic fault. These findings contribute to a nuanced understanding of coseismic landslide susceptibility and offer valuable insights for future Newmark method-based coseismic landslide displacement calculations.

Keywords: 2022 Luding earthquake; coseismic landslide susceptibility; Newmark displacement regression model; distance to the seismogenic fault; epicentral distance

Citation: Liu, T.; Zang, M.; Peng, J.; Xu, C. Evaluating Coseismic Landslide Susceptibility Following the 2022 Luding Earthquake: A Comparative Analysis of Six Displacement Regression Models Integrating Epicentral and Seismogenic Fault Distances within the Permanent-Displacement Framework. *Remote Sens.* **2024**, *16*, 2675. https://doi.org/10.3390/rs16142675

Academic Editor: Salvatore Stramondo

Received: 9 June 2024
Revised: 9 July 2024
Accepted: 16 July 2024
Published: 22 July 2024

1. Introduction

Coseismic landslides are geological events where a rock or soil mass, which is approaching or is already at a critical state, experiences premature sliding triggered by an earthquake [1]. Coseismic landslides pose immense hazards, sometimes surpassing the damage caused by earthquakes themselves. In recent years, the occurrence of powerful earthquakes worldwide, such as the 2008 Wenchuan earthquake (Ms8.0), the 2010 Yushu earthquake (Ms7.1), the 2018 Indonesia earthquake (Ms7.4), and the 2023 Turkey

earthquake (Ms7.8), has drawn significant attention to the evaluation of coseismic landslide susceptibility. This has become a critical and challenging issue in the academic and engineering fields.

According to the China Earthquake Networks Center (https://news.ceic.ac.cn/, last access: 15 June 2023), on 5 September 2022, a magnitude 6.8 earthquake occurred in Moxi Town, Luding County, Ganzi Tibetan Autonomous Prefecture, Sichuan Province, southwestern China. The epicenter was located at 29.59°N, 102.08°E, with a focal depth of 16 km. This earthquake triggered numerous landslides in mountainous areas, resulting in a total of 93 fatalities and 20 people missing, as well as enormous economic losses [2]. Considering the immense hazards posed by coseismic landslides, conducting a regional analysis of the susceptibility to such events is of vital significance for post-disaster reconstruction and ensuring people's well-being.

The commonly used methods for analyzing regional susceptibility to coseismic landslides can be roughly categorized into three types: the engineering geological analysis method, the statistical regression analysis method, and the mechanical analysis method. The engineering geological analysis method is a comprehensive qualitative method based on an understanding of slope stability and engineering experience. In the early stages of landslide research, due to the limitations of research methods and the complex geological conditions of slopes, this method was commonly used for evaluating the seismic stability of slopes [3]. The statistical regression method is based on analyzing factors that influence the development of coseismic landslides, summarizing regularities, and making predictions. By summarizing the distribution patterns of post-coseismic landslides and studying the relationships between landslides and seismic parameters as well as other influencing factors, the susceptibility trends of coseismic landslides can be extrapolated based on established statistical patterns [4–7]. The mechanical modeling method is based on the principles of mechanics, involving analyzing the instability mechanism and sliding process of slopes to quantitatively characterize mechanical or kinematic parameters. It provides a basis for the analysis of seismic landslide susceptibility and has clear physical significance.

In the context of mechanical model analysis, Terzaghi first proposed the pseudo-static method [8]. This method simplifies seismic motion by treating it as a constant body force acting on the potential sliding mass during static limit equilibrium calculations. However, the pseudo-static method has its limitations. It assumes constant pseudo-static forces and assesses stability but does not predict failure when safety factors fall below 1. Additionally, it has difficulty determining minimum safety factors and pinpointing the exact location of the sliding surface during landslide movement under specific conditions [9–12]. Clough and Chopra introduced the finite element method into the analysis of soil dynamic response, signifying the introduction of numerical analysis methods into the field of dynamic response analysis of slopes [13]. However, numerical analysis methods also have certain limitations. They require significant computational resources and time, and defining the model scope and boundary conditions can be challenging. Consequently, these methods are typically employed for analyzing individual slopes [14]. Newmark's cumulative displacement method is a highly classical approach to the analysis of physical mechanics. Newmark introduced this method based on a rigid block model to compute the permanent displacements of slopes under seismic forces, thereby assessing slope stability under seismic conditions [15]. Based on the 1994 Northridge earthquake in California, Jibson et al. pioneered the application of the Newmark model to regional seismic landslide susceptibility assessment [16,17]. Their research significantly advanced the utilization and development of the Newmark method in the field of regional seismic landslide susceptibility analysis. Subsequently, a series of simplified Newmark displacement analysis methods based on mechanical models have been applied to seismic landslide hazard assessments in various regions, including the 2008 Wenchuan earthquake [18], the 2013 Lushan earthquake [19], the 2014 Ludian earthquake [20,21], and the 2022 Luding earthquake [22]. The Newmark method remains one of the most widely used international approaches for evaluating seismic landslide hazards.

In the Newmark method, the permanent displacement value is obtained by double-integrating the time during which the seismic acceleration exceeds the critical acceleration of the slope [15]. In the regional analysis process, it is often necessary to rasterize the study area using GIS techniques. Therefore, it is not practical to calculate the permanent displacement values for each grid cell using the standard Newmark method. To address this issue, some scholars have studied the relationship between Newmark permanent displacement and seismic motion parameters, establishing simple and practical mathematical regression models for the rapid prediction of seismic landslide susceptibility in regional analyses. Ambraseys and Menu were the first to conduct such research [23]. They selected 50 sets of strong ground motion records from 11 earthquakes and proposed a relationship between Newmark permanent displacement D_n and the ratio of slope critical acceleration a_c to PGA. Jibson proposed a relationship between D_n and Arias intensity (I_a), a_c, based on 11 strong earthquake records. Later, in 1998 and 2000, this formula was improved using 555 strong earthquake records from 13 seismic events [16,17,24]. However, the majority of the selected earthquake data in this model had relatively small peak ground acceleration, leading to distorted results when the critical acceleration was larger. Therefore, Jibson selected 2270 strong earthquake records from 30 global seismic events and fitted regression formulas for displacement with different combinations of seismic motion parameters [25]. Subsequently, several scholars derived displacement regression formulas with various parameter combinations based on different seismic motion records, such as a_c, the ratio of a_c to PGA, PGA, peak ground velocity (PGV), and I_a [26–29]. These regression formulas facilitate using the Newmark model in the susceptibility assessment of coseismic landslides. However, some issues should be addressed. The determination of these regression formulas is specific to certain geological backgrounds and particular seismic events. Therefore, their applicability should be validated rather than solely considering the number of factors or the size of the database.

We obtained a comprehensive inventory of landslides caused by the 2022 Luding earthquake. In this paper, we will summarize six types of displacement regression models, choosing the best-fitting model by comparing the predicted displacement with the inventory of actual landslides. The impact of parameters on the fitting of regression models is also explored. Finally, a hazard map of landslides posed by the Luding earthquake is provided using the best-fitting regression model.

2. Study Area

The study area is located at the intersection of Ganzi Autonomous Prefecture and Ya'an City in the northwest of Sichuan Province, China (Figure 1). The area covers approximately 964.8 km^2 and includes the epicenter, the seismogenic fault, and most of the landslides triggered by the 2022 Luding earthquake. The elevation ranges from 874 to 4668 m, with the highest point situated on the Wanglangbao mountain in the central-left part of the area and the lowest point in the valley of the Daduhe River in the central area. The Daduhe River flows through the study area from north to south and is characterized by deep valleys, developed tributaries, and steep slopes on both sides. Deep valleys also contribute to slope instability. The vertical relief between the valley bottoms and the mountain ridges can create significant pressure on the slopes. Additionally, the rapid changes in elevation within a short distance can cause stress concentration, making the slopes more vulnerable to failure. The predominant lithologies in the study area vary in age from the Paleoproterozoic to the Mesozoic, including diorite and picrite of the Paleoproterozoic; rhyolite porphyry and granite of the Sinian Formation; limestone, dolomite, and slate of the Devonian; quartzite, dolomite, and limestone of the Permian; sandstone of the Triassic; and conglomerate of the Quaternary period. The distribution of lithologies is shown in Figure 2.

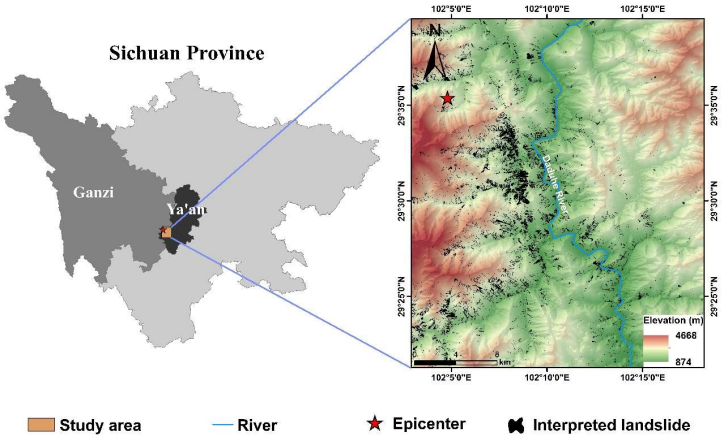

Figure 1. Map of the study area showing the inventoried landslides.

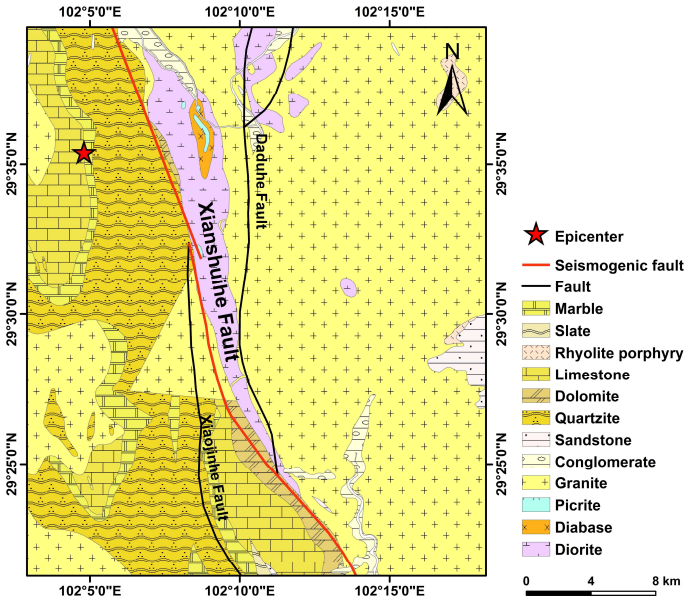

Figure 2. Geological map of the study area showing lithology and faults. The fault data are from the Seismic Active Fault Survey Data Center (https://www.activefault-datacenter.cn/, last access: 11 May 2023).

The seismogenic fault of the Luding earthquake is the Moxi fault, the southern section of the Xianshuihe fault zone, which is the boundary between the Sichuan–Yunnan Block and the Bayan Har Block [30]. The Xianshuihe fault system serves as the northeast boundary fault of the material extrusion from the Qinghai–Tibet Plateau to the southeast and is one of the most active fault systems in China's continental interior [31,32]. The left-lateral strike–slip fault motion is decomposed onto other adjacent fault zones, such as the Anning River, Dalingshan, and Zemu River fault zones, in the eastern region. The left-lateral shearing strike–slip motion then occurs along the Xiaojianghe fault zone and extends into Yunnan, crossing the well-known Red River fault and extending into Myanmar.

3. Materials and Methodology

3.1. Sources of Data

The required data primarily include a digital elevation model (DEM) of the study area, details on the lithology and its physical–mechanical parameters, and information on PGA and PGV that describe seismic effects. The slope of the study area was extracted from the DEM using basic slope algorithms on a GIS platform. Using empirical formulas, the seismic

parameter I_a was fitted based on the distance to the seismogenic fault and lithology [33]. The sources of data are listed in Table 1.

Table 1. Sources of data required for the calculation.

Characteristic Factor	Spatial Resolution	Source
Elevation	30 m	Geospatial Data Cloud—SRTM1 (https://www.gscloud.cn/, last access: 23 June 2023)
Lithology	1:200,000	National Geological Data Museum (https://www.ngac.cn/, last access: 23 June 2023)
PGA	\	United States Geological Survey (USGS) (https://www.usgs.gov, last access: 23 June 2023)
PGV	\	United States Geological Survey (USGS) (https://www.usgs.gov, last access: 23 June 2023)
Fault	\	Seismic Active Fault Survey Data Center (https://www.activefault-datacenter.cn/, last access: 11 May 2023)

3.2. Inventory of the Landslides Induced by the 2022 Luding Earthquake

An accurate and detailed compilation database of landslides serves as the foundation for a susceptibility assessment of coseismic landslides. Therefore, we employed a combined approach of visual interpretation based on optical satellite imagery and field investigations to establish a landslide catalog [34]. The optical satellite imagery used in this study was obtained from Planet satellite data, captured in July 2022 and 29 September 2022. Contrasting high-resolution remote sensing images before and after the earthquake enables the creation of a landslide inventory, and field investigations can further optimize the boundaries of landslides. The distribution of the interpreted coseismic landslides is illustrated in Figure 1.

3.3. Methodology

In 1965, Newmark proposed a model that conceptualizes a sliding mass in nature as a rigid body sliding on a slope (Figure 3). The model evaluates the stability of soil and rock masses by calculating the permanent cumulative displacement of the soil and rock masses under seismic actions. The rigid body itself has a critical acceleration, which represents the minimum seismic acceleration required for the rigid body to overcome the shear resistance and start sliding. The stability of the slope is related to the a_c of the sliding mass, and a_c can be expressed as:

$$a_c = (F_S - 1)g \sin \alpha \quad (1)$$

where a_c is the critical acceleration, F_S is the safety factor, g is the gravitational acceleration, and α can be expressed as the slope angle of the sliding block.

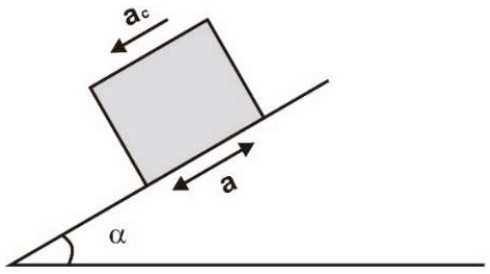

Figure 3. Sliding-block model used for the Newmark analysis [17].

The safety factor can be determined by the model's infinite slope limit equilibrium equation:

$$F_S = \frac{c'}{\gamma t \sin \alpha} + \frac{\tan \varphi'}{\tan \alpha} + \frac{m\gamma_w \tan \varphi'}{\gamma \tan \alpha} \quad (2)$$

where c' represents the effective internal cohesion, γ represents the bulk density of the sliding block, t represents the thickness of the sliding block, α represents the slope angle of the sliding block, φ' represents the effective internal friction angle, m represents the water content of the sliding block, and γ_w represents the bulk density of water.

In this case, if an external load acceleration is applied to the sliding block, the difference between the external load acceleration and the critical acceleration can be integrated (Figure 4A) to obtain the sliding velocity of the sliding block (Figure 4B). Integrating the velocity will yield the cumulative displacement of the sliding mass (Figure 4C). The stability of the slope is determined by the magnitude of the displacements.

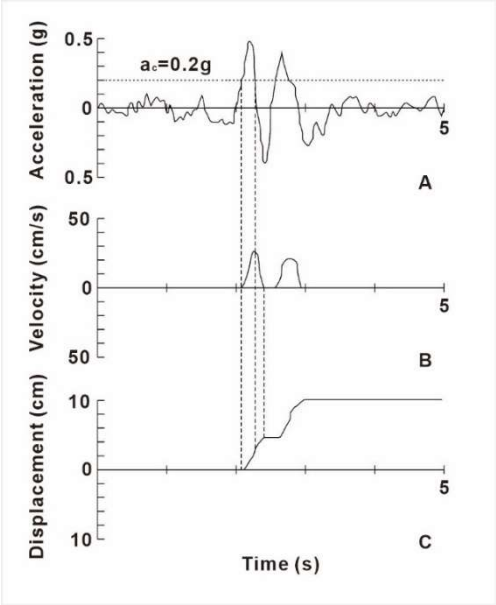

Figure 4. Demonstration of the Newmark analysis algorithm [17]. (**A**) Earthquake acceleration-time history with critical acceleration (horizontal dashed line) of 0.20 g superimposed. (**B**) Velocity of landslide block versus time. (**C**) Displacement of landslide block versus time.

4. Results and Analysis

4.1. Static Factor-of-Safety Map

In this study, a 30 m × 30 m digital elevation model (DEM) was selected from the Geospatial Data Cloud (https://www.gscloud.cn/search, last access: 23 June 2023), and a slope map of the study area was generated from the DEM using the GIS platform (Figure 5). The static safety factor can be calculated using Equation (2), where the first term on the right-hand side of Equation (2) represents the cohesion of the landslide mass, and the thickness of the sliding mass is empirically taken as 3 m. The second term represents the frictional component, while the third term represents the decrease in the frictional strength of the slope due to the pore pressure of water. The study area did not experience significant rainfall before the earthquake; the influence of pore water pressure is not considered when calculating the static safety factor in this study [22]. Only the effects of material cohesion and internal friction angle on the safety factor are considered. The rock types and their physical–mechanical parameters in the study area are shown in Table 2. According to the Newmark model, a smaller static safety factor indicates a more unstable slope. However, when calculating the a_c, any parts where the static safety factor is less than 1 will result in a negative a_c. Therefore, in this study, the parts where the static safety factor is less than 1 are all defined as 1.01, just slightly above the limit equilibrium state, to avoid negative a_c [16,17]. According to Keefer's research, the minimum slope angle for most coseismic landslides is 5° [1]. The areas with slope angles less than 5° had very high safety factors during the Luding earthquake and will not be considered in the calculation. The resulting static safety factor ranges from 1 to 13.6, as shown in Figure 6.

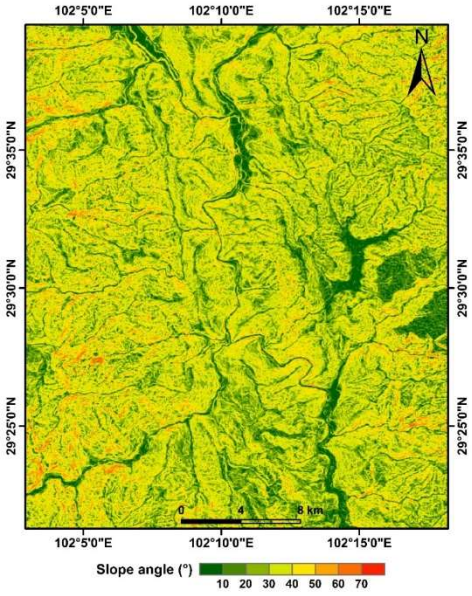

Figure 5. Slope map derived from the DEM of the study area.

Table 2. Physical and mechanical parameters of rocks in the study area.

Rock Type	c'/MPa	φ'/°	γ/kN·m^{-3}
Dolomite	0.036	43	25.9
Slate	0.011	28	26.5
Marble	0.051	31	26.4
Granite	0.031	35	26.1
Limestone	0.030	45	21.5
Diabase	0.010	24.5	27.5
Picrite	0.045	50	31.3
Conglomerate	0.034	35	21.5
Rhyolite porphyry	0.035	33	25
Sandstone	0.025	42	26.5
Diorite	0.040	50	26.9
Quartzite	0.037	40	26

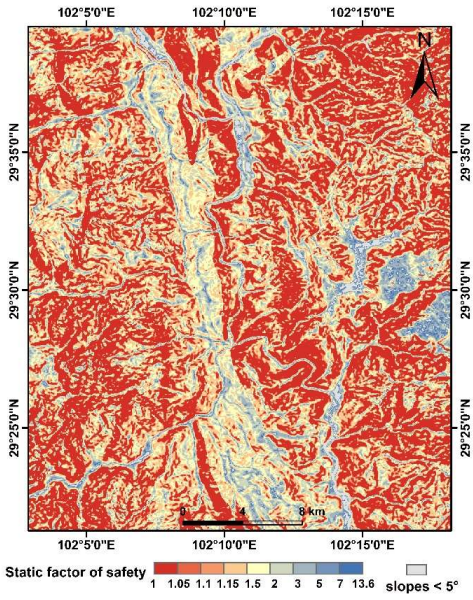

Figure 6. Static factor-of-safety map of the study area.

The safety factor is primarily associated with regional rock strength and terrain data, as is evident from Figure 6. It can be observed that the safety factor in the mountainous regions on both sides of the study area is lower compared to the river valley plain area in the middle. This can be further corroborated by comparing it with the slope map (Figure 5), where areas with higher slopes exhibit lower safety factors, indicating greater danger.

4.2. Critical Acceleration Map

According to the Newmark method, the a_c of potential sliding masses can be analyzed through a pseudo-static analysis of the static safety factor and the regional slope angle. The spatial distribution map of a_c (Figure 7) is calculated using Equation (1). The a_c of the sliding mass is determined by the topography and lithology of the mass, independent of the seismic shaking induced by earthquakes. Therefore, the spatial distribution map of a_c illustrates the sensitivity of coseismic landslides [16,17]. Lower values of a_c indicate greater susceptibility to a coseismic landslide.

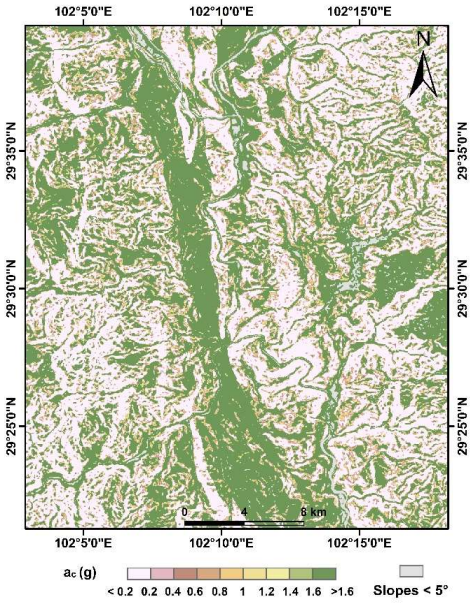

Figure 7. Map showing a_c in the study area.

4.3. Predicted Displacement Map

4.3.1. Seismic Motion Map

The seismic parameters widely used in the Newmark model primarily include PGA, PGV, and I_a. The maps of PGA and PGV were obtained from the USGS, with the epicenter of the Luding earthquake reported to be at a latitude of 29.679°N and a longitude of 102.236°E. However, according to the China Earthquake Networks Center (CENC) and our field investigations, the actual epicenter of the Luding earthquake was at a latitude of 29.59°N and a longitude of 102.08°E (https://news.ceic.ac.cn). We utilized a GIS platform to calculate the relative deviation between the actual epicenter and the erroneous epicenter. Furthermore, we spatially transformed PGA and PGV data downloaded from USGS based on the geographic displacement between the two epicenters. The calibrated PGA distribution map and PGV distribution map are shown in Figure 8a,b, respectively. The PGA range is from 0.1 g to 0.46 g, while the PGV range is from 8 m/s to 52 m/s. I_a is mainly obtained through empirical attenuation formulas based on the relationship between earthquake magnitude, epicentral distance, and distance from the seismogenic fault. Several scholars have fitted attenuation formulas for different parameters based on seismic records [35,36].

In this study, we chose the empirical attenuation formula for I_a developed by Wang et al. based on the analysis of 40 strong-motion records from southwestern China [36]:

$$\log I_a = -2.96 \log(D_f + 42) + 6.39 \quad (3)$$

where D_f is the distance from the seismogenic fault.

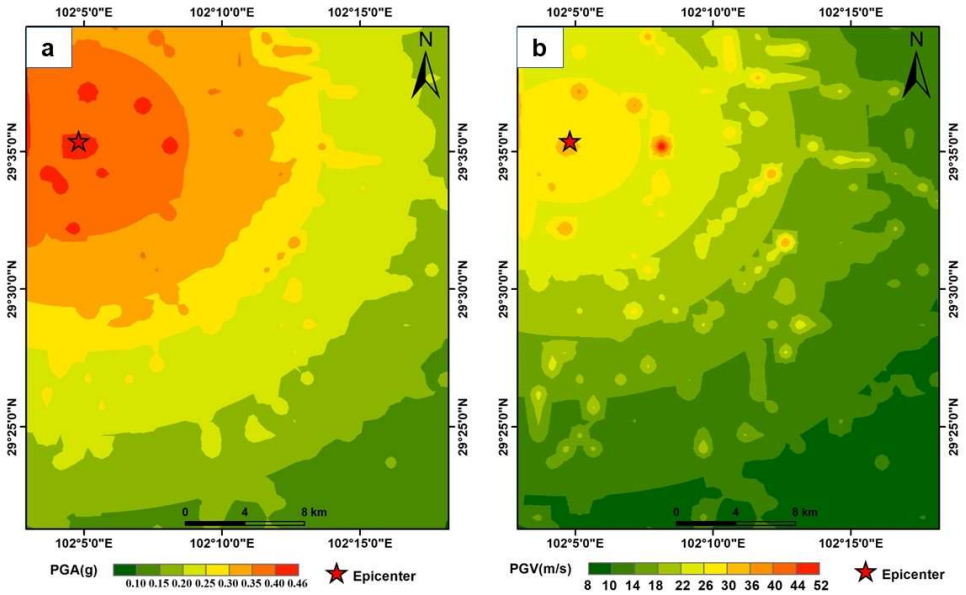

Figure 8. Contour map of seismic motion produced by the Luding earthquake. (**a**) PGA and (**b**) PGV.

It is important to emphasize that the attenuation formula yields a total value of I_a from north–south and east–west directions, while PGA and PGV are the average values in these two horizontal directions. To facilitate comparison, we divided I_a by two to obtain an average value in the horizontal direction. The resulting distribution map of I_a is shown in Figure 9, with a maximum value of 19.24 m/s and a minimum value of 5.93 m/s.

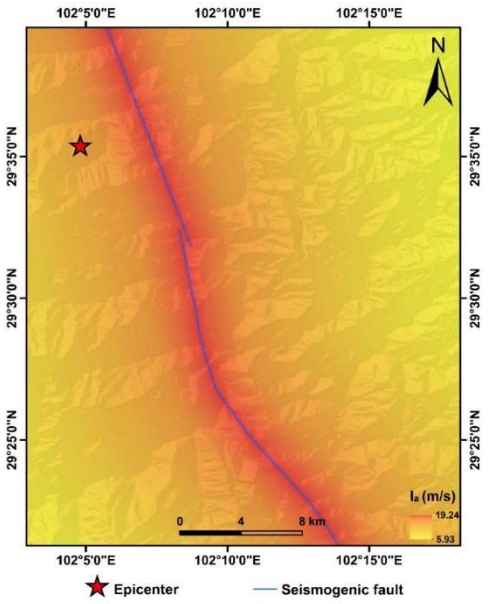

Figure 9. Contour map of I_a produced by the Luding earthquake in the study area.

4.3.2. Newmark Displacement Map

The Newmark permanent displacement is calculated by performing a double integration of the seismic acceleration that exceeds the slope's critical acceleration over time. In regional analysis, it is unfeasible to apply the standard Newmark method to compute permanent displacement for individual grid cells. To solve this problem, many scholars have studied the relationship between Newmark permanent displacement and seismic motion parameters, establishing some simple and practical mathematical regression models for the rapid prediction of seismic landslide susceptibility at the regional scale [16,17,23,25–29]. The ratio of a_c to PGA is referred to as the acceleration ratio (AR). The mathematical regression formula for Newmark permanent displacement can be categorized into six types based on the parameter combinations: (1) AR; (2) a_c and I_a; (3) AR and I_a; (4) AR and PGA; (5) AR, PGA, and PGV; (6) AR, PGA, PGV, and I_a.

For each type, in accordance with previous studies, the Newmark displacement regression formula with the highest coefficient of determination (R^2) was selected to compare the fitting degree between the predicted displacements and the distribution of landslides triggered by the 2022 Luding earthquake. The specific regression formulas are shown in Table 3.

Table 3. Newmark displacement equations for different parameter combinations.

Combination of Ground Vibration Parameters	Equation		References
AR	$\log D_n = 0.194 + \log\left[\left(1 - \frac{a_c}{PGA}\right)^{2.262}\left(\frac{a_c}{PGA}\right)^{-1.754}\right] \pm 0.371,$	(4)	Xu et al. [28]
a_c, I_a	$\log D_n = 0.465 \log I_a + 12.896 a_c \log I_a - 22.201 a_c + 2.092 \pm 0.148,$	(5)	Jin et al. [29]
AR, I_a	$\log D_n = 0.405 \log I_a - 4.756 \frac{a_c}{PGA} + 2.276 \pm 0.423,$	(6)	Xu et al. [28]
AR, PGA	$\ln D_n = 5.52 - 4.43\left(\frac{a_c}{PGA}\right) - 20.39\left(\frac{a_c}{PGA}\right)^2 + 42.61\left(\frac{a_c}{PGA}\right)^3 - 28.74\left(\frac{a_c}{PGA}\right)^4 + 0.72 \ln PGA,$	(7)	Saygili et al. [26]
AR, PGA, PGV	$\ln D_n = -1.56 - 4.58\left(\frac{a_c}{PGA}\right) - 20.48\left(\frac{a_c}{PGA}\right)^2 + 44.75\left(\frac{a_c}{PGA}\right)^3 - 30.50\left(\frac{a_c}{PGA}\right)^4 - 0.64 \ln PGA + 1.55 \ln PGV,$	(8)	Saygili et al. [26]
AR, PGA, PGV, I_a	$\ln D_n = -0.74 - 4.93\left(\frac{a_c}{PGA}\right) - 19.91\left(\frac{a_c}{PGA}\right)^2 + 43.75\left(\frac{a_c}{PGA}\right)^3 - 30.12\left(\frac{a_c}{PGA}\right)^4 - 1.30 \ln PGA + 1.04 \ln PGV + 0.67 \ln I_a,$	(9)	Saygili et al. [26]

The Newmark permanent displacement distribution was computed using six distinct regression equations, as depicted in Figure 10. The high-displacement zone, determined by Equation (5), predominantly spans both sides of the seismogenic fault, with the extent of this zone diminishing further away from the fault (Figure 10b). The remaining five calculations show similar characteristics: the low-displacement zone is primarily distributed in the plains on both sides of the Daduhe River valley, while the high-displacement zone is mainly distributed near the epicenter and on the steep slopes on both sides of the fault. However, unlike the distribution of the static safety factor (Figure 6) and critical acceleration (Figure 7), Newmark displacements show a distribution of displacements on the northwest side of the study area that are greater than those on the southeast side. In other words, the level of danger is higher on the northwest side compared to the southeast side. This can be attributed to the fact that the epicenter of the Luding earthquake is located on the northwest side of the study area; thus, the Newmark displacement distribution pattern for the Luding earthquake prediction, as depicted in Figure 10, reflects the influence of seismic action on slope stability.

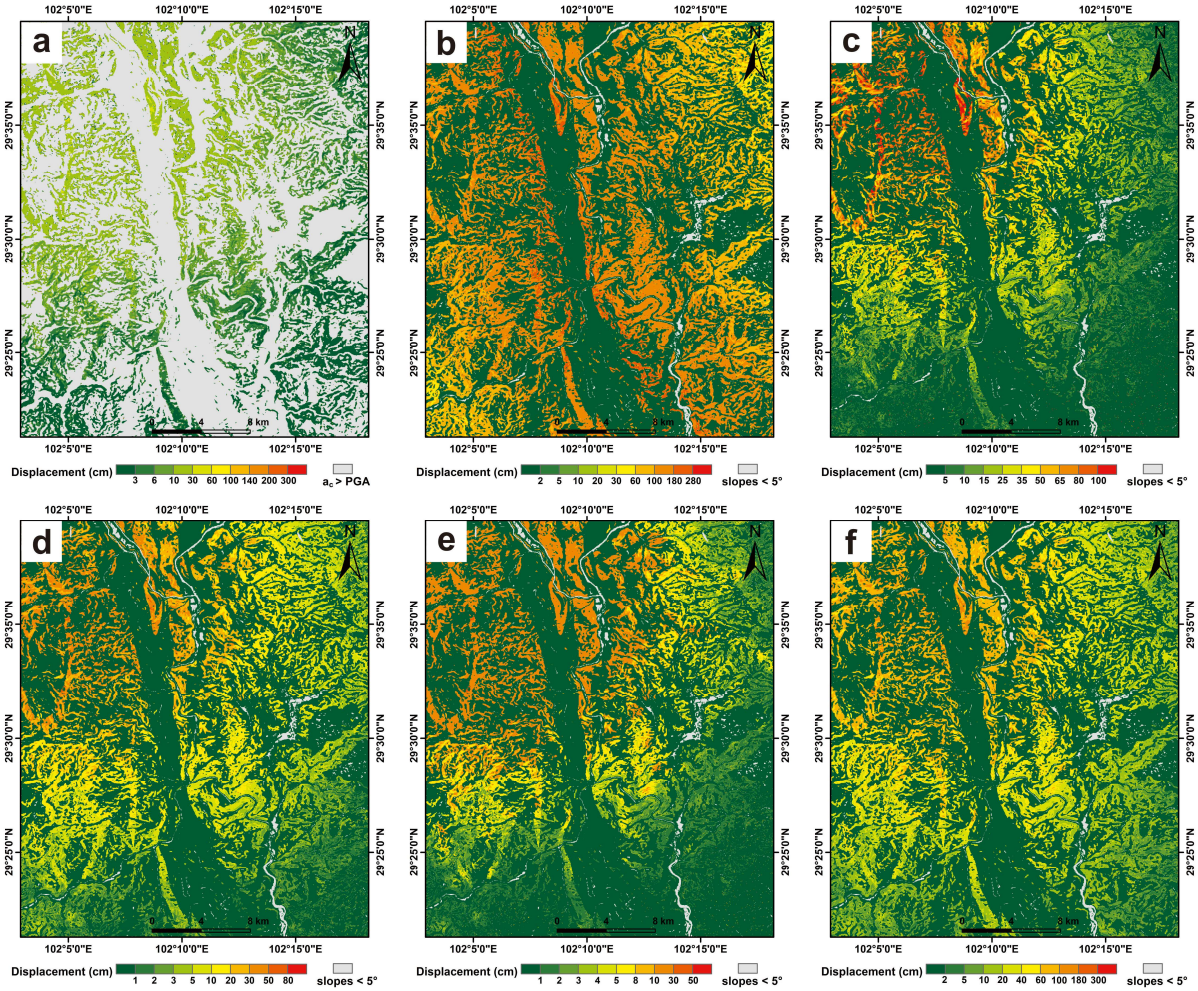

Figure 10. Map showing the displacements predicted by different fitting formulas for the study area. (**a**) Calculated by Equation (4); (**b**) Calculated by Equation (5); (**c**) Calculated by Equation (6); (**d**) Calculated by Equation (7); (**e**) Calculated by Equation (8); (**f**) Calculated by Equation (9).

4.4. Comparative Analysis of Regression Models

The area under the receiver operating characteristic (ROC) curve (AUC) served as a measure of the fitting degree. An AUC value less than or equal to 0.5 indicates a model fit worse than random prediction, while an AUC value of 1.0 indicates a perfect fit with the landslide distribution [7]. By plotting the ROC curve using these values, the fit of the six models can be compared. The displacement values obtained from the calculation model can be divided into intervals according to the natural breakpoints. By arranging the intervals in descending order based on their areas as a proportion of the total area, the x-axis can be defined. Similarly, the y-axis can be defined by arranging the intervals in descending order based on the proportion of landslide area within each interval as a proportion of the total study area landslide area. Figure 11 demonstrates that the regression equation proposed by Saygili et al. [26], incorporating four parameters—i.e., AR, PGA, PGV, and I_a (Equation (9))—exhibits the highest degree of fit to the coseismic landslides, with an AUC value of 0.61.

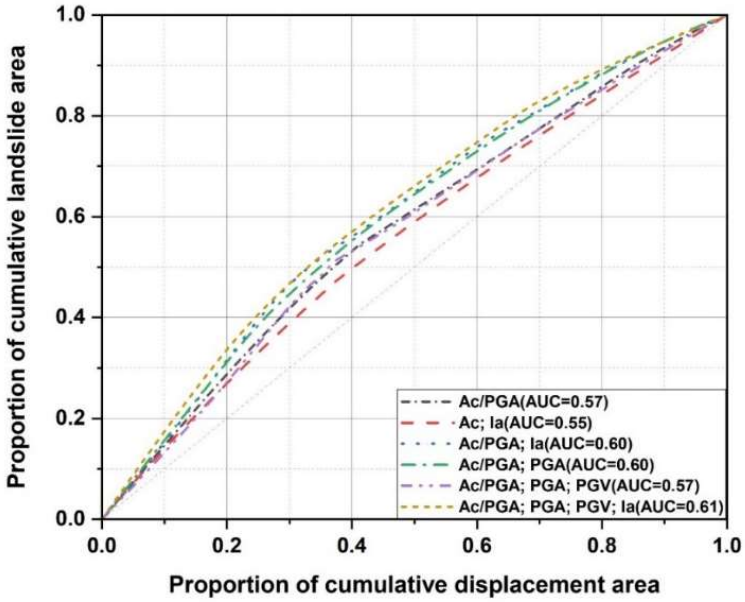

Figure 11. Comparison of area under the ROC curve for six different displacement formulas.

Jibson et al. employed the Weibull curve to fit the calculated results of the Newmark method with the actual landslide distribution and found a good fit between the curve and the data [16,17]. Therefore, in this study, the Weibull curve was adopted to fit the Newmark displacement with the actual landslide distribution. The principle involves rasterizing the calculated displacements, using the proportion of actual landslide cells ($P(f)$) within each displacement interval plotted on the y-axis and the endpoint of each displacement interval on the x-axis, and fitting the data points with the Weibull curve. The displacement values computed under six different regression equations were fitted to the Weibull function, and the final fitting equations, along with their respective correlation coefficients, are presented in Table 4. It should be noted that the regression equation proposed by Saygili [26], which includes four parameters, achieved the highest correlation coefficient (R^2 = 0.87) when fitting the displacement values to the Weibull function (Equation (15)). This finding is consistent with the results of the AUC analysis, leading this study to conclude that Equation (9) demonstrates the highest fitting accuracy with respect to the distribution of earthquake-induced landslides.

Table 4. The Weibull fitting formula under different parameter combinations.

Combination of Ground Vibration Parameters	Equation		R^2
AR	$P(f) = 0.054\left(1 - e^{-0.61{D_n}^{0.73}}\right)$,	(10)	0.87
a_c, I_a	$P(f) = 1.47\left(1 - e^{-0.029{D_n}^{0.04}}\right)$,	(11)	0.79
AR, I_a	$P(f) = 0.074\left(1 - e^{-0.32{D_n}^{0.41}}\right)$,	(12)	0.80
AR, PGA	$P(f) = 0.094\left(1 - e^{-0.38{D_n}^{0.3}}\right)$,	(13)	0.80
AR, PGA, PGV	$P(f) = 0.07\left(1 - e^{-0.47{D_n}^{0.6}}\right)$,	(14)	0.83
AR, PGA, PGV, I_a	$P(f) = 13.8\left(1 - e^{-0.002{D_n}^{0.21}}\right)$,	(15)	0.87

4.5. Spatial Probability of Coseismic Landslides

Figure 12 shows the Weibull function fitted using the results computed from Equation (9). As the displacement increases, the proportion of actual landslides within the displacement interval also increases, indicating a larger landslide-to-displacement ratio. After 200 cm, this ratio stabilizes, with a maximum proportion of approximately 8.6%. Reflecting the fitted

curve data onto the study area yields a spatial probability distribution map of coseismic landslides (Figure 13), where the majority of landslides are located in the high-hazard areas (indicated with a red color). This demonstrates that the distribution map effectively represents the hazardous zones of coseismic landslides.

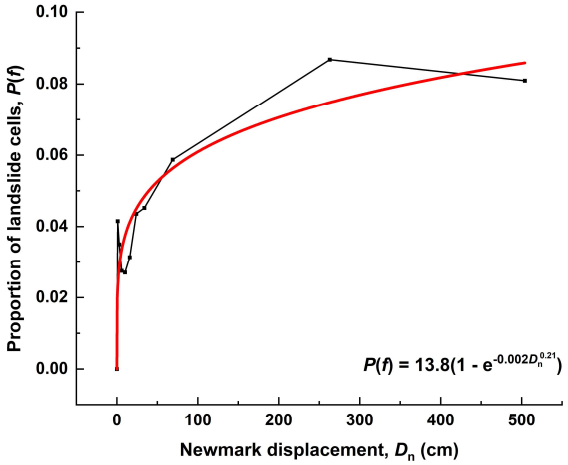

Figure 12. Proportion of landslide cells as a function of Newmark displacement (Equation (15)). Each dot represents the proportion of a Newmark displacement bin; the red line is the fitting curve of the data using a modified Weibull function.

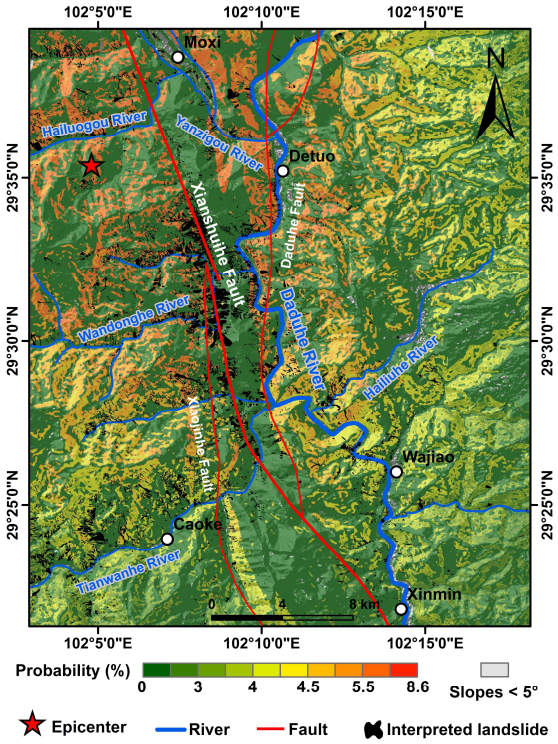

Figure 13. Map showing the spatial probability distribution of seismic landslides obtained from the Newmark model, which has the best fit to the actual landslide distribution.

5. Discussion

Figure 13 shows that the higher probability areas of coseismic landslides are mainly located at Moxi and Detuo. The overall northwestern part of the study area poses a greater hazard of coseismic landslides compared to the southeastern part, which is consistent with the findings of Liu et al. [22]. The higher probability areas, where landslides are prone

to occur, are concentrated along the Xianshuihe fault belt (Figure 13), which indicates that the seismogenic fault plays an important role in determining the spatial distribution of coseismic landslides [37]. The areas with a higher probability of coseismic landslides are also concentrated in steep slopes on both sides of the Daduhe, Yanzigou, Hailuogou, and Wandonghe valleys (Figure 13). Greater slope gradients significantly increase the occurrence of coseismic landslides.

In our calculations, the upper Moxi and Detuo regions of the study area are identified as high-susceptibility zones for coseismic landslides, despite the actual occurrence of few landslides in these regions. A comparison with Figures 2 and 5 reveals that Moxi and Detuo regions are characterized by large areas of loose Quaternary deposits but relatively gentle slope degrees. The low rock strength contributes to high-susceptibility designation for coseismic landslides based on the Newmark method. However, in reality, smooth Quaternary deposits are not particularly susceptible to coseismic landslides, which may explain the discrepancy between our calculations and the actual landslide distribution. Jibson et al. indicated that slopes steeper than a certain angle remain unstable even at high strengths [16,17]. Therefore, Zang et al. assigned an angle of $45^\circ + \varphi/2$ to slopes steeper than 60° to avoid overestimating the susceptibility of coseismic landslides in a Newmark analysis [21]. Our findings suggest that significant differences in rock strength between types have a substantial effect on the model output. Another issue that needs attention is the presence of low-susceptibility zones on the local eastern side of the Xianshuihe fault, attributed to the high rock strength of quartzite and diorite. However, coseismic landslides are still observed in these zones. Despite the relatively high rock strength, the proximity to the seismogenic fault results in a highly fractured rock mass, significantly reducing its overall strength. The stability of rock slopes is closely correlated with rock mass strength rather than just rock strength, a factor that the Newmark model fails to adequately consider. This discrepancy leads to a mismatch between the calculated results and the actual distribution of coseismic landslides in these regions. Future assessments of coseismic landslide susceptibility should pay more attention to the influence of rock structure.

Among the six different regression models, the model proposed by Saygili et al. [26]—which utilized AR, PGA, PGV, and I_a—achieved the highest AUC value and exhibited a good fit with the distribution of the landslides induced by the 2022 Luding earthquake. However, this is not solely attributed to the number of seismic parameters used in the model, as Saygili et al. achieved an AUC value of 0.57 with their three-parameter model (AR, PGA, and PGV), whereas Xu et al. obtained a higher AUC value of 0.60 with their two-parameter model (AR and I_a) [26,28]. Therefore, the number of seismic parameters in the model is not the primary factor contributing to its good fit with actual landslides. This study suggests that the reason behind the good fit of the four-parameter model lies in the correlation between the distribution of PGA and PGV (Figure 8a,b) and the epicentral distance, as well as the correlation between the distribution of I_a (Figure 9) and the distance to the seismogenic fault. Similarly, Xu et al. achieved the second-highest AUC value with their two-parameter model (AR and I_a), which also incorporated PGA and I_a [26,28]. Both models considered the influence of epicentral distance and the distance to the seismogenic fault on seismic parameters, resulting in a good fit with the actual distribution of coseismic landslides. Therefore, it can be indicated that considering both epicentral distance and the distance to the seismogenic fault when incorporating seismic parameters in the Newmark model has a favorable impact on the prediction results.

To enhance our understanding of the influence exerted by epicentral distance and the distance to the seismogenic fault on the spatial distribution of coseismic landslides, we conducted a comparative study. Figure 14 shows that the density of coseismic landslides reaches its peak near the Xianshuihe fault, followed by an approximately monotonic decrease as the distance to the seismogenic fault increases. When the distance to the seismogenic fault reaches 15 km, the density of coseismic landslides diminishes to nearly zero. Conversely, landslides are seldom distributed in the vicinity of the epicenter, with their prevalence peaking as the epicentral distance extends to 7 km. Subsequently, the

density of coseismic landslides exhibits a fluctuating decrease with further increases in epicentral distance, ultimately approaching zero at an epicentral distance of 35 km. It is deduced that when the predicted region encompasses or is in close proximity to the seismogenic fault, precedence should be given to the influence of the distance to the seismogenic fault, followed by the impact of the epicentral distance. Conversely, when the predicted region is situated far from the seismogenic fault, the fault's influence on coseismic landslides becomes less pronounced. In such instances, the distribution density of coseismic landslides is primarily influenced by the epicentral distance, with additional considerations required for factors such as lithology and topography. This finding is consistent with the results obtained by other scholars who studied the 2008 Wenchuan earthquake, the 2013 Lushan earthquake, and the 2014 Ludian earthquake [37–39].

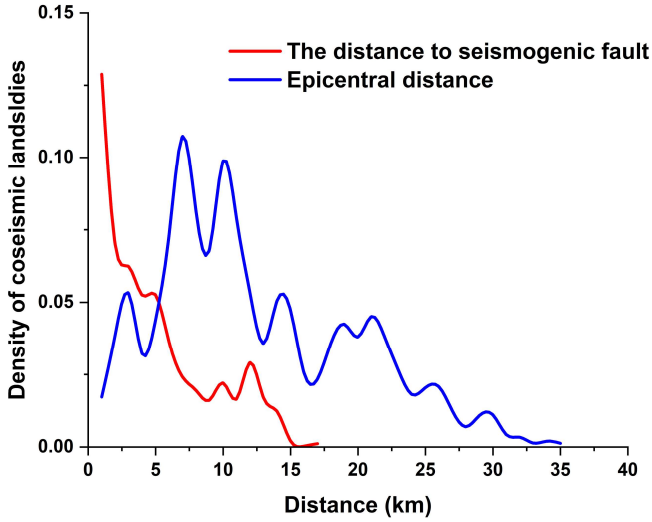

Figure 14. Map showing the change in landslide density with increasing distance from the epicenter and the seismogenic fault.

In the study by Jin et al., Equation (5) and Equation (7) were compared using data from the 2013 Lushan Ms7.0 earthquake [29]. It was found that Equation (5) exhibited a significantly smaller root mean square error compared to Equation (7). However, in the present investigation, Equation (5) yielded the lowest AUC value of 0.55, diverging from the findings reported by Jin et al. This discrepancy can be attributed to the approach employed by Jin et al. [29], where Equation (5) was fitted to the seismic records by inputting a_c values within the range from 0.01 to 0.15 in increments of 0.01. The model coefficients were subsequently readjusted based on these standardized values. Notably, this process overlooked the consideration of region-specific critical accelerations influenced by lithology and topography. In contrast, our study validated the model results using the actual distribution of landslide occurrences, resulting in outcomes differing from those reported by Jin et al. [29]. Consequently, it is recommended that future coseismic hazard assessments employing the Newmark method should involve the refitting of model coefficients based on historical earthquake data specific to the study area. Subsequent displacement predictions using the revised model are crucial for obtaining accurate and region-specific results.

When computing permanent displacement using the Newmark displacement regression formula, Equation (4), in a regional analysis [28], only the grid cell where PGA is greater than a_c is taken into account. This precaution is taken due to the model's formula violating mathematical laws, resulting in a negative value in the logarithmic component when considering the grid cell where a_c exceeds PGA (Table 3). However, this rationale is consistent with the principles of the Newmark method. As the Newmark displacement originates from the double integration of the segment where PGA exceeds a_c [15], the following question arises: should a similar procedure be applied when employing alternative Newmark displacement regression formulas for regional analysis, focusing solely on grid

cells where PGA surpasses a_c? To address this question, we conducted a comparative analysis using the Newmark displacement regression formula with the highest degree of fit (Equation (9)). In one scenario, calculations were performed exclusively for grid cells in the region where PGA exceeds a_c, assuming stability and no sliding for other grid cells. In the second scenario, computations were carried out for all grid cells in the region, regardless of whether the PGA in a particular grid cell exceeded a_c or not. Simultaneously, the magnitude of the AUC values was employed to compare the accuracy of the two calculation methods. The results indicated that when exclusively considering the grid cells where a_c is smaller than PGA, the resulting AUC value was 0.6094, whereas, without imposing this condition, the model yielded an AUC value of 0.6092. It can be deduced that this condition exerts a negligible impact on the overall calculation. Nevertheless, in practical coseismic landslide occurrences, some landslides do take place in the grid cells where a_c exceeds PGA. Although the calculated displacement values for these grid cells in the theoretical model are relatively small, they still pose a certain level of hazard. Relying solely on calculations that consider the grid cells where PGA is greater than a_c might not accurately predict hazardous areas. Therefore, it is advisable to omit this condition when utilizing Newmark displacement regression models for calculation to obtain more comprehensive and reliable results.

As mentioned in the introduction section, statistical analysis is also an important method for assessing the susceptibility to coseismic landslides. Previous studies have shown that slope gradient and the distance to the seismogenic fault are two important factors influencing the distribution density of coseismic landslides [37,38]. Research conducted by Jibson et al. has demonstrated that the Newmark method adeptly delineates the impact of slope gradient on the spatial distribution of coseismic landslides [16,17]. The study presented in this paper demonstrates that the epicentral distance and the distance to the seismogenic fault can influence the predictive performance of the Newmark method, thereby affecting the accuracy of coseismic landslide susceptibility assessments. Constrained by the seismic parameter data obtained, the distribution of PGA and PGV appears in concentric circular shapes, without reflecting the influence of the seismogenic fault. This somewhat diminishes the impact of the distance to the seismogenic fault on the Newmark method, resulting in a decrease in the AUC value. Continuous improvement through subsequent research endeavors is required to address this limitation. Furthermore, the study area selected in this paper does not revolve around the epicenter but rather centers on the seismogenic fault. Additionally, efforts were made to encompass as many interpreted coseismic landslides as possible. However, this approach may not objectively reflect the influence of the epicentral distance on the assessment outcomes of coseismic landslide susceptibility, thus contributing to the relatively modest AUC values observed. From the foregoing discussion, it is evident that the selection of fundamental data, such as terrain and seismic parameters, significantly impacts the assessment accuracy of the Newmark method. This amplifies the complexity of its application and underscores the need for dedicated analysis and special consideration in future applications.

6. Conclusions

This study conducted a susceptibility assessment of coseismic landslides triggered by the 2022 Luding Ms6.8 earthquake using six different Newmark displacement regression models, and explored the factors affecting the applicability of the models. The main conclusions are as follows:

(1) The 2022 Luding earthquake induced 13,759 landslides within an area of 964.8 km^2. These landslides were predominantly concentrated along steep mountain slopes on both sides of the fault and in the valley area on the right bank of the Daduhe River. The prediction outcomes designate Moxi Town, Detuo Town, both sides of the Daduhe River, Wandonghe River, Hailuogou River, and Yanzigou River as high-susceptibility areas for coseismic landslides.

(2) The model composed of seismic parameters such as AR, PGA, PGV, and I_a demonstrates a commendable fit to the distribution of coseismic landslides. Conversely, models that solely account for a_c and I_a yield unsatisfactory fitting results. Consequently, when employing the Newmark displacement method for assessing susceptibility to coseismic landslides, it becomes imperative to validate the fitting formula, taking into account the specific geological and environmental conditions.

(3) In the proximity of the fault, priority should be given to considering the influence of the distance to the seismogenic fault and epicentral distance when assessing the susceptibility to coseismic landslides. However, when situated far from the fault, the impact of distance to the seismogenic fault on landslides diminishes. In such cases, attention should be directed towards factors like epicentral distance, topography, and lithology, which become more significant in influencing susceptibility.

Author Contributions: Conceptualization, M.Z. and J.P.; methodology, T.L. and M.Z.; validation, T.L.; formal analysis, T.L. and M.Z.; investigation, T.L.; resources, M.Z. and C.X.; data curation, M.Z.; writing—original draft preparation, T.L. and M.Z.; writing—review and editing, M.Z., J.P. and C.X.; project administration, M.Z. and J.P.; funding acquisition, M.Z. All authors have read and agreed to the published version of the manuscript.

Funding: This research was funded by the National Natural Science Foundation of China (grant nos. 42207215 and 41825018).

Data Availability Statement: The original contributions presented in the study are included in the article; further inquiries can be directed to the corresponding authors.

Acknowledgments: The authors thank the National Natural Science Foundation of China (Grant Nos. 42207215 and 41825018). We also appreciate the insightful comments from the reviewing experts and academic editor, which significantly enhanced the quality of this manuscript.

Conflicts of Interest: The authors declare no competing interests.

References

1. Keefer, D.K. Landslides caused by earthquakes. *Geol. Soc. Am. Bull.* **1984**, *95*, 406–421. [CrossRef]
2. Fan, X.M.; Wang, X.; Dai, L.X.; Fang, C.Y.; Deng, Y.; Zou, C.B.; Tang, M.G.; Wei, Z.L.; Dou, X.Y.; Zhang, J.; et al. Characteristics and spatial distribution pattern of M S 6.8 Luding earthquake occurred on September 5, 2022. *J. Eng. Geol.* **2022**, *30*, 1504–1516.
3. Sun, Y.K.; Mou, H.C.; Yao, B.K. *Slope Stability Analysis*; Science Press: Beijing, China, 1988.
4. Parise, M.; Jibson, R.W. A seismic landslide susceptibility rating of geologic units based on analysis of characteristics of landslides triggered by the 17 January, 1994 Northridge, California earthquake. *Eng. Geol.* **2000**, *58*, 251–270. [CrossRef]
5. Marzorati, S.; Luzi, L.; De, A.M. Rock falls induced by earthquakes: A statistical approach. *Soil Dyn. Earthq. Eng.* **2002**, *22*, 565–577. [CrossRef]
6. Wang, Y.Q.; Gao, Y.P.; Xin, H.B. A research on prediction of seismic stability of slopes by grey clustering method. *Ind. Constr.* **2002**, *32*, 44–47.
7. Miles, S.B.; Keefer, D.K. Evaluation of CAMEL—Comprehensive areal model of earthquake-induced landslides. *Eng. Geol.* **2009**, *104*, 1–15.
8. Terzaghi, K. Mechanism of Landslides. In *Application of Geology to Engineering Practice*; Paige, S., Ed.; Geological Society of America: Boulder, CO, USA, 1950.
9. Seed, H.B. *Stability of Earth and Rockfill Dams during Earthquakes*; Wiley (John) and Sons: Hoboken, NJ, USA, 1973.
10. Jibson, R.W. Methods for assessing the stability of slopes during earthquakes—A retrospective. *Eng. Geol.* **2011**, *122*, 43–50.
11. Wu, X.Y.; Law, K.T.; Selvadural, A.S. Examination of the pseudo-static limit equilibrium method for dynamic stability analysis of slopes. In Proceedings of the 44th Canadian Geotechnical Conference, Calgary, AB, Canada, 29 September–2 October 1991; pp. 1961–1968.
12. Ling, H.I.; Cheng, A.H. Rock sliding induced by seismic force. *Int. J. Rock Mech. Min. Sci.* **1997**, *34*, 1021–1029.
13. Clough, R.W.; Chopra, A.K. Earthquake stress analysis in earth dams. *J. Eng. Mech. Div.* **1966**, *92*, 197–211.
14. Zang, M.D. *A probabilistic Framework for Mapping Hazards of Coseismic Landslides*; University of Chinese Academy of Sciences: Beijing, China, 2019.
15. Newmark, N.M. Effects of earthquakes on dams and embankments. *Geotechnique* **1965**, *15*, 139–160.
16. Jibson, R.W.; Harp, E.L.; Michael, J.A. *A Method for Producing Digital Probabilistic Seismic Landslide Hazard Maps: An Example from the Los Angeles, California, Area*; US Department of the Interior, US Geological Survey: Washington, DC, USA, 1998.
17. Jibson, R.W.; Harp, E.L.; Michael, J.A. A method for producing digital probabilistic seismic landslide hazard maps. *Eng. Geol.* **2000**, *58*, 271–289.

18. Wang, T.; Wu, S.R.; Shi, J.S.; Xin, P. Case study on rapid assessment of regional seismic landslide hazard based on simplified Newmark displacement model: Wenchuan Ms 8.0 earthquake. *J. Eng. Geol.* **2013**, *21*, 16–24.
19. Chen, X.L.; Yuan, R.M.; Yu, L. Applying the Newmark's model to the assessment of earthquake-triggered landslides during the Lushan earthquake. *Seismol. Geol.* **2013**, *35*, 661–670.
20. Chen, X.L.; Liu, C.; Wang, M. A method for quick assessment of earthquake-triggered landslide hazards: A case study of the Mw6. 1 2014 Ludian, China earthquake. *Bull. Eng. Geol. Environ.* **2019**, *78*, 2449–2458. [CrossRef]
21. Zang, M.D.; Qi, S.W.; Zou, Y.; Sheng, Z.P.; Blanca, S.Z. An improved method of Newmark analysis for mapping hazards of coseismic landslides. *Nat. Hazards Earth Syst. Sci.* **2020**, *20*, 713–726. [CrossRef]
22. Liu, J.M.; Wang, T.; DU, J.J.; Chen, K.; Huang, J.H.; Wang, H.J.; Ruan, Q.Q.; Feng, F. Emergency rapid assessment of landslides induced by the Luding MS6.8 earthquake in Sichuan of China. *Hydrogeol. Eng. Geol.* **2023**, *50*, 84–94.
23. Ambraseys, N.N.; Menu, J.M. Earthquake-induced ground displacements. *Earthq. Eng. Struct. Dyn.* **1988**, *16*, 985–1006.
24. Jibson, R.W. Predicting earthquake-induced landslide displacements using Newmark's sliding block analysis. *Transp. Res. Rec.* **1993**, *1411*, 9–17.
25. Jibson, R.W. Regression models for estimating coseismic landslide displacement. *Eng. Geol.* **2007**, *91*, 209–218.
26. Saygili, G.; Rathje, E.M. Empirical predictive models for earthquake-induced sliding displacements of slopes. *J. Geotech. Geoenviron. Eng.* **2008**, *134*, 790–803.
27. Rathje, E.M.; Saygili, G. Probabilistic assessment of earthquake-induced sliding displacements of natural slopes. *Bull. N. Z. Soc. Earthq. Eng.* **2009**, *42*, 18–27. [CrossRef]
28. Xu, G.X.; Yao, L.K.; Li, C.H.; Wang, X.F. Predictive models for permanent displacement of slopes based on recorded strong-motion data of Wenchuan earthquake. *Chin. J. Geotech. Eng.* **2012**, *34*, 1131–1136.
29. Jin, J.L.; Wang, Y.; Gao, D.; Yuan, R.M.; Yang, X.Y. New evaluation models of Newmark displacement for Southwest China. *Bull. Seismol. Soc. Am.* **2018**, *108*, 2221–2236.
30. Yang, Z.; Dai, D.; Zhang, Y.; Zhang, X.M.; Liu, J. Rupture process and aftershock focal mechanisms of the 2022 M6. 8 Luding earthquake in Sichuan. *Earthq. Sci.* **2022**, *35*, 474–484.
31. Zhang, P.Z. Current Tectonic Deformation, Strain Distribution and Deep Dynamic Process in the Western Sichuan of the Eastern Margin of the Tibetan Plateau. *Sci. China (Ser. D)* **2008**, *38*, 1041–1056.
32. Bai, M.K.; Chevalier, M.L.; Li, H.B.; Pan, J.W.; Wu, Q.; Wang, S.G.; Liu, F.C.; Jiao, L.Q.; Zhang, J.J.; Zhang, L.; et al. Late Quaternary slip rate and earthquake hazard along the Qianning segment, Xianshuihe fault. *Acta Geol. Sin.* **2022**, *96*, 2312–2332.
33. Wang, X.Y.; Wang, D.W. Relationships between the Wenchuan earthquake-induced landslide and peak ground velocity, Sichuan, China. *Geol. Bull. China* **2011**, *30*, 159–165.
34. Shao, X.Y.; Ma, S.Y.; Xu, C.; Xie, C.C.; Li, T.; Huang, Y.D.; Huang, Y.; Xiao, Z.K. Landslides triggered by the 2022 Ms. 6.8 Luding strike-slip earthquake: An update. *Eng. Geol.* **2024**, *335*, 107536.
35. Xie, J.J.; Wen, Z.P.; Gao, M.T.; Hu, J.X.; He, S.L. Characteristics of near-fault vertical and horizontal ground motion from the 2008 Wenchuan earthquake. *Chin. J. Geophys.* **2010**, *53*, 555–565.
36. Wang, X.Y.; Nie, G.Z.; Ma, M.J. Evaluation model of landslide hazards induced by the 2008 Wenchuan earthquake using strong motion data. *Earthq. Sci.* **2011**, *24*, 311–319.
37. Zou, Y.; Qi, S.W.; Guo, S.F.; Zheng, B.W.; Zhan, Z.F.; He, N.W.; Huang, X.L.; Hou, X.K.; Liu, H.Y. Factors controlling the spatial distribution of coseismic landslides triggered by the Mw 6.1 Ludian earthquake in China. *Eng. Geol.* **2022**, *296*, 106477. [CrossRef]
38. Qi, S.W.; Xu, Q.; Lan, H.X.; Zhang, B.; Liu, J.Y. Spatial distribution analysis of landslides triggered by 2008.5. 12 Wenchuan Earthquake, China. *Eng. Geol.* **2010**, *116*, 95–108. [CrossRef]
39. Li, G.; Zang, M.D.; Qi, S.W.; Bo, J.S.; Yang, G.X.; Liu, T.H. An Infinite Slope Model Considering Unloading Joints for Spatial Evaluation of Coseismic Landslide Hazards Triggered by a Reverse Seismogenic Fault: A Case Study of the 2013 Lushan Earthquake. *Sustainability* **2024**, *16*, 138. [CrossRef]